

Collective quantum stochastic resonance in Rydberg atoms

Haowei Li,^{1,*} Konghao Sun,^{1,*} and Wei Yi^{1,2,3,†}

¹CAS Key Laboratory of Quantum Information, University of Science and Technology of China, Hefei 230026, China

²CAS Center For Excellence in Quantum Information and Quantum Physics, Hefei 230026, China

³Hefei National Laboratory, University of Science and Technology of China, Hefei 230088, China

We study the collective response of a group of dissipative Rydberg atoms to a periodic modulation of the Rydberg excitation laser. Focusing on the emergent collective-jump dynamics, where the system stochastically switches between states with distinct Rydberg excitations, we show that the counting statistics of the state switching is qualitatively changed by the periodic drive. The impact is most prominent when the driving frequency is comparable to the emergent collective-jump rate, as the jumps tend to synchronize with the external drive, and their counting statistics exhibits a series of suppressed subharmonics of the driving frequency. These phenomena are manifestations of a novel type of stochastic resonance, where a cooperative collective state switching is facilitated by quantum fluctuations in a many-body open system. Such a collective quantum stochastic resonance further leads to an enhanced signal-to-noise ratio in the power spectrum of the Rydberg excitations, for which the synchronized collective jumps are viewed as the output signal. We confirm the many-body quantum nature of the resonance by devising a cluster model, under which the role of many-body correlations is analyzed by changing the size of the atom clusters.

Introduction. Stochastic resonance describes the counter-intuitive signal amplification by adding an appropriate dose of noise [1, 2]. Originally suggested to explain the recurring ice ages [3], stochastic resonance proves to be a universal phenomenon in nature, appearing also in biological processes [4, 5], and across a variety of physical systems ranging from optics [6–11] to electronics [12, 13]. The occurrence of stochastic resonance generally entails a noisy bistable system periodically modulated by a weak signal. When the frequency of the driving signal and the noise strength are appropriate, the response of the system exhibits resonance-like behaviors, including the synchronization of the bistable-state switching with the external drive, and an enhanced signal-to-noise ratio (SNR). While stochastic resonances are predominantly found in non-linear systems with classical noise, they also emerge in quantum mechanical settings, assisted by quantum fluctuations [14–18]. These quantum stochastic resonances have only recently been observed in quantum-dot microstructures [19] and scanning tunneling microscopes [20], where the intrinsic fluctuations of single-electron tunneling play a key role.

But quantum fluctuations, particularly those in many-body open systems, also manifest in collective dynamics. Take a group of dissipative Rydberg atoms for instance. The atomic ground states therein are laser-coupled to high-lying energy levels with significant principle quantum number n , but subject to spontaneous decay back to the ground state. An outstanding feature of the Rydberg atoms is the strong long-range interactions, which are central to the recent advances in quantum computation and simulation with Rydberg atoms [21–29]. Previous studies have shown that the entanglement generated by the long-range interactions, combined with the repetitive quantum measurements (in the form of spontaneous emission), lead to collective quantum jumps between two metastable many-body states with high and low Rydberg excitations, respectively [30]. Since these emergent collective jumps are a manifestation of quantum fluctuations in a many-

body open system, it is tempting to ask whether a quantum stochastic resonance can be engineered based on them.

In this work, we reveal such a quantum stochastic resonance in the counting statistics of the collective jumps in a group of Rydberg atoms, where the Rydberg excitation laser is subject to a periodic modulation. Viewing the periodic drive as the input signal and the collective jumps the system response, we find that, when the driving frequency is comparable to the intrinsic collective-jump rate, the jumps tend to synchronize with the input signal, and a series of subharmonics emerge in the counting statistics, reminiscent of a conventional stochastic resonance. As a definitive signature of the resonance [1], a maximum SNR in the power spectrum of the Rydberg excitations is observed at what we identify as the resonance point. At the resonance point, the subharmonics become suppressed and an optimum synchronization of the collective-state switching with the driving frequency is achieved. Importantly, unlike the stochastic resonance in classical non-linear systems, or in quantum stochastic resonances featuring single-particle tunneling, many-body correlations and collective jumps are indispensable for the collective quantum stochastic resonance reported here. We explicitly demonstrate this by adopting a cluster model where quantum coherence and entanglement are only retained within each atom cluster, while the inter-cluster interactions are treated on the mean-field level. As the size of the clusters decreases, both the counting statistics and the resonance condition change dramatically, culminating in the eventual disappearance of the collective jumps and resonance signatures when the model is reduced to a classical one with non-linear interactions.

Emergent collective jumps in Rydberg atoms. We consider a group of N atoms uniformly subject to a Rydberg excitation laser. As illustrated in Fig. 1(a), the ground state of the j th atom $|g_j\rangle$ is continuously coupled to a Rydberg state $|r_j\rangle$. The Rydberg state has a finite lifetime, which can be further tuned through additional couplings to other excited states. Approximating the Rydberg atoms as an ensemble of two-level

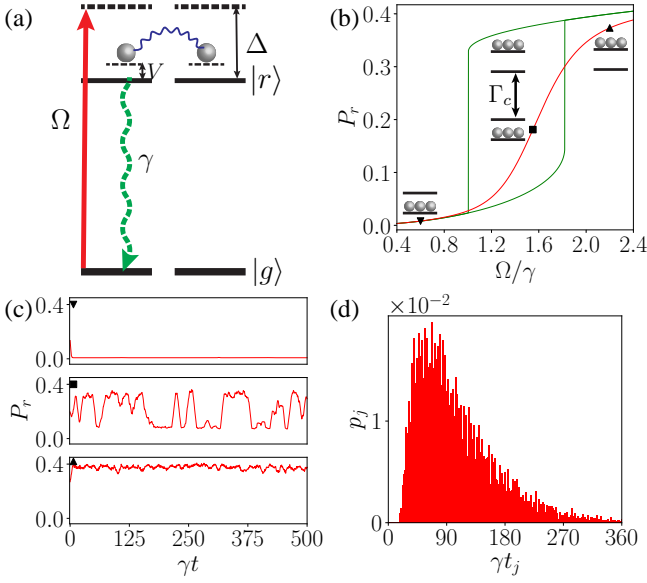


FIG. 1. (a) Schematic illustration of the level scheme. The Rydberg excitation laser couples the atomic ground state $|g\rangle$ and a Rydberg state $|r\rangle$. Atoms in the excited state interact with each other through the Rydberg long-range interaction, and can spontaneously decay back to the ground state. (b) Rydberg-state population P_r in the steady state of the master equation (red), and in the bistable states of the optical Bloch equations (green). Collective jumps with rate Γ_c (defined in the main text) predominantly occur in the mean-field bistable region, but only visible through quantum trajectories. Here the mean-field bistable region exists in the range $\Omega/\gamma \in [1.00, 1.82]$. (c) Rydberg excitation along a single trajectory. From top to bottom: $\Omega/\gamma = 0.6, 1.55, 2.2$, consistent with the corresponding black markers in (b). (d) Normalized distribution p_j of inter-jump intervals, indicative of the counting statistics of the collective jumps in the middle panel of (c). We take $\gamma\delta t = 2$ for the definition of p_j and t_j (see main text for details). For numerical calculations, we take $\Delta/\gamma = 3.4$, $(N-1)V/\gamma = 10$, and $N = 8$ in all figures.

systems and neglecting the much slower external motion, the dissipative dynamics of the density matrix ρ is depicted by the Lindblad master equation

$$\dot{\rho} = -i[H, \rho] + \gamma \sum_j \left(-\frac{1}{2} \{L_j^\dagger L_j, \rho\} + L_j \rho L_j^\dagger \right), \quad (1)$$

with the Hamiltonian

$$H = \sum_j \left[-\frac{\Delta}{2} (\sigma_j^z + 1) + \frac{\Omega}{2} \sigma_j^x \right] + \frac{V}{4} \sum_{j < k} (\sigma_j^z + 1) (\sigma_k^z + 1). \quad (2)$$

The quantum jump operator $L_j = (\sigma_j^x - i\sigma_j^y)/2$ describes the spontaneous decay of the j th atom back to its ground state, with a decay rate γ . Here Ω is the Rabi frequency of the Rydberg excitation laser, Δ is its detuning, and $\sigma_j^{x,y,z}$ are the Pauli operators associated with the two-dimensional subspace spanned by $\{|g_j\rangle, |r_j\rangle\}$ of the j th atom, with $\sigma_j^z = |r_j\rangle\langle r_j| - |g_j\rangle\langle g_j|$. For simplicity, we model the long-range Rydberg interactions using a constant all-to-all coupling. Note

that all the key results still hold when we consider the spatial dependence of the Rydberg interactions [31].

The driven-dissipative Rydberg system features a unique steady state (with density matrix ρ^s), which can be solved by setting $\dot{\rho}^s = 0$ in Eq. (1). In Fig. 1(b), we show the steady-state Rydberg excitation $P_r = \rho_{rr}^s$ for $N = 8$ atoms (red). For later discussions, it is instructive to compare the steady-state solution from the master equation with those under a mean-field approximation. In the latter case, the interatomic correlations are neglected, the density matrices of individual atoms become decoupled through $\rho = \bigotimes_j \bar{\rho}$, and the dynamics of $\bar{\rho}$ is governed by the optical Bloch equations [30, 32]

$$\dot{\bar{\rho}}_{rr} = -\Omega \text{Im} \bar{\rho}_{rg} - \gamma \bar{\rho}_{rr}, \quad (3)$$

$$\dot{\bar{\rho}}_{rg} = i \left[\Delta - (N-1)V\bar{\rho}_{rr} \right] \bar{\rho}_{rg} - \frac{\gamma}{2} \bar{\rho}_{rg} + i\Omega \left(\bar{\rho}_{rr} - \frac{1}{2} \right), \quad (4)$$

where the Rydberg interactions contribute toward a density-dependent effective detuning. Steady-state solutions can be obtained by setting $\dot{\bar{\rho}} = 0$ in the equations above, giving rise to the green lines in Fig. 1(b). Notably, a bistable region emerges, where the two steady-state solutions feature high and low Rydberg excitations, respectively. The bistability derives from the non-linear interaction terms under the mean-field approximation, and is well-studied in thermal Rydberg gases [33–35]. While such a bistability is absent in the full-quantum description of Eq. (1), its quantum correspondence nevertheless manifests in the counting statistics of the open-system dynamics.

To see this, we unravel the density-matrix dynamics into an ensemble of quantum trajectories [36–38]. In a given time interval $[t, t + \Delta t]$ along each trajectory, the many-body wave function $|\psi(t)\rangle$ undergoes the quantum jump $|\psi(t)\rangle \rightarrow L_j |\psi(t)\rangle$ with a probability $\gamma \Delta t \langle \psi(t) | L_j^\dagger L_j | \psi(t) \rangle$, or evolves under a non-Hermitian effective Hamiltonian $H_{\text{eff}} = H - i\frac{\gamma}{2} \sum_j L_j^\dagger L_j$ with the probability $1 - \gamma \Delta t \sum_j \langle \psi(t) | L_j^\dagger L_j | \psi(t) \rangle$. The state is then normalized to repeat the process for the following time interval. Physically, each single trajectory simulates the wavefunction evolution in a single-run experiment where a single random quantum jump corresponds to the spontaneous emission of a single photon by an atom.

An important feature of an individual quantum trajectory of the system is the possible emergence of collective jumps between metastable many-body states with high and low Rydberg excitations. As discussed in Ref. [30], the two states are characterized by the joint emissions or non-emissions of individual atoms, and the collective jumps between them originate from the interplay of Rydberg interaction and dissipation. In Fig. 1(c), we show the single-trajectory evolution of the Rydberg excitation $P_r = \frac{1}{2} \langle \psi(t) | \sum_j (\sigma_j^z + 1) | \psi(t) \rangle$ with different Ω . Apparently, when the parameters are within the mean-field bistable region [Fig. 1(c) middle panel], P_r switches between two plateaus, whose values correspond to the bistable steady-state solutions under the mean-field approximation. When the system is tuned away from the bistable region, the collective

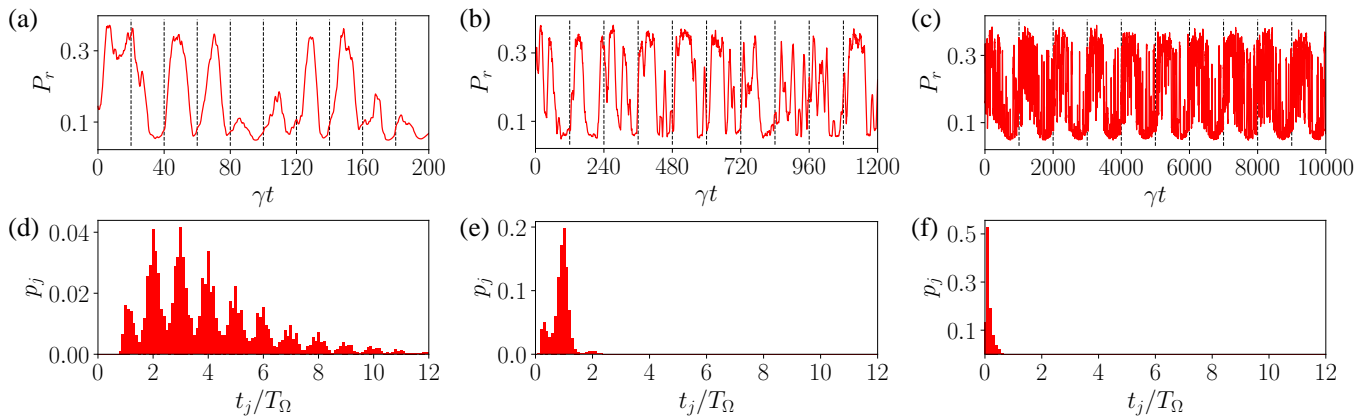


FIG. 2. (a)(b)(c) Single-trajectory dynamics of the Rydberg excitation P_r under a periodic drive. (d)(e)(f) Distribution of inter-jump intervals for a single trajectory within the evolution time $\gamma t \in [0, 10^6]$. The driving parameters are $\Omega_0/\gamma = 1.55$, $A_\Omega/\gamma = 0.2$, and (a)(d) $\gamma T_\Omega = 20$, (b)(e) $\gamma T_\Omega = 120$, (c)(f) $\gamma T_\Omega = 1000$. For all figures, we take $N = 8$ and $\delta t = 0.1T_\Omega$. Other parameters are the same as those in Fig. 1.

jumps dramatically decrease in frequency, and eventually vanish in effect [Fig. 1(c) top and bottom panels]. This is the case when the steady-state solution of the master equation is close to one of the steady-state solutions of the optical Bloch equations.

To characterize the counting statistics of the collective jumps, we plot the distribution of inter-jump intervals in Fig. 1(d). To define the distribution, we uniformly discretize the overall evolution time T into small segments of δt . We then count the number of adjacent downward collective jumps n_j that occur within the time interval $[t_j - 0.5\delta t, t_j + 0.5\delta t]$, where $t_j = j\delta t$. Here the downward collective jumps are the state switching from high to low Rydberg excitations. The normalized distribution for the inter-jump interval is defined as $p_j = n_j / \sum_j n_j$, which represents the probability for adjacent downward collective jumps to occur within the corresponding time interval. The distribution shows an exponential decay for large j , suggesting the stochastic nature of the jumps. We can further define a collective-jump rate $\Gamma_c = \sum_j n_j / T$, which represents an emergent many-body energy scale for the driven-dissipative system.

Counting statistics and quantum stochastic resonance. We now consider the counting statistics of the collective jumps in response to a periodic modulation of the Rydberg excitation laser. Specifically, we consider a time-periodic Rabi frequency $\Omega(t) = \Omega_0 + A_\Omega \cos(2\pi t/T_\Omega)$, where T_Ω and A_Ω are respectively the driving period and amplitude, and Ω_0 is the time-independent Rabi frequency.

In Fig. 2(a)(b)(c), we show the time-evolved Rydberg excitations of single trajectories under different driving frequencies. The occurrence of the collective jumps appear to be regulated by the driving frequency, distinct from the more random pattern in Fig. 1(c). Importantly, at an appropriate intermediate driving frequency, the collective jumps fully synchronize with the drive [see Fig. 2(b)]. Such a pattern is more visible from the counting statistics of the jumps, shown in Fig. 2(d)(e)(f). When the driving period is small, the

response of the system, in terms of the downward collective-jump intervals, features a series of subharmonics of the driving frequency [see Fig. 2(d)]. On increasing the driving period, the subharmonics become suppressed, and the distribution is peaked at $t_j/T_\Omega = 1$, indicating full synchronization [see Fig. 2(e)]. Under a very long driving period, more than one jumps can occur within one driving period, and p_j is peaked at $t_j/T_\Omega = 0$ [see Fig. 2(f)]. In all cases, the distribution of p_j exhibits discrete peaks centered at integer t_j/T_Ω , in sharp contrast to the pattern in Fig. 1(d) without the periodic drive.

The synchronization of the system's response with the periodic drive is reminiscent of the stochastic resonance, where the resonance condition is qualitatively understood as the matching between the external driving frequency and the rate of the emergent collective jumps [1, 19, 39]. To confirm such an observation, we calculate the SNR of the collective jumps, which is an outstanding quantifier for the stochastic resonance. For this purpose, we view the period modulation as a weak input signal, and the collective jumps the output. The SNR can be extracted from the power spectrum $P(f)$ of the collective jumps in a single trajectory, where $P(f)$ is the square of the Fourier transform of $P_r(t)$. The SNR is defined as [2]

$$\text{SNR}_{\text{dB}} = 10 \log_{10} \left[\frac{P(f = \frac{1}{T_\Omega})}{\frac{1}{f_{\text{max}} - f_{\text{min}}} \int_{f_{\text{min}}}^{f_{\text{max}}} P(f) df} \right], \quad (5)$$

where the frequency range $[f_{\text{min}}, f_{\text{max}}]$ of the noise-power integral is typically taken close to but not over the driving frequency. To compensate for the arbitrariness in the choice of $f_{\text{min}, \text{max}}$, at any given point, we take three different sets of ranges: $[f_{\text{min}}, f_{\text{max}}] \in (1/T_\Omega)\{[0.25, 0.75], [1.25, 1.75], [2.25, 2.75]\}$, and retain the one with the largest integrated noise power.

We plot the numerically evaluated SNR in Fig. 3(a), as a function of the driving period, where the SNR is further aver-

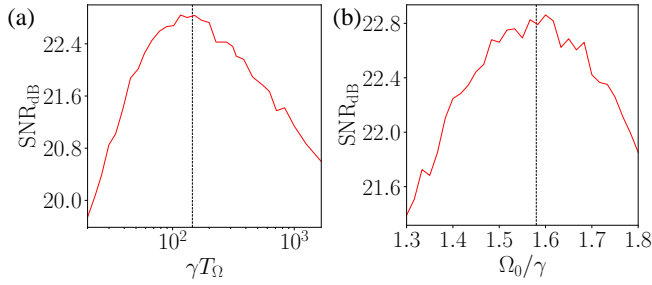


FIG. 3. (a) Trajectory-averaged SNR, with a fixed $\Omega_0/\gamma = 1.55$, $A_\Omega/\gamma = 0.2$, and varying T_Ω . (b) SNR as a function of Ω_0 with fixed $T_\Omega = 144.2$ and $A_\Omega/\gamma = 0.2$. The vertical dashed lines in both subplots indicate the theoretically predicted resonance condition $T_c \tilde{\Gamma}_c = 1$, which gives $\gamma T_c \approx 145.4$ in (a), and $\Omega_0/\gamma \approx 1.58$ in (b). Here $\tilde{\Gamma}_c$ is the downward collective-jump rate that is numerically averaged along the driving path [31]. For both calculations here, we take a single-trajectory evolution time of $\gamma t = 10000$, and average over 100 trajectories. Other parameters are the same as those in Fig. 1.

aged over many trajectories for better convergence within the numerically feasible evolution time. The resonance point is identified as the peak location in the SNR, which is close to the theoretically predicted resonance point $T_c \tilde{\Gamma}_c = 1$ [1, 39] (vertical dashed line). Here $\tilde{\Gamma}_c$ is estimated using the averaged collective-jump rate along the driving path $\Omega(t)$ [31], since Γ_c depends on the value of Ω and changes along the path [see also Fig. 4(a)]. The general behavior of the SNR can be understood in view of the distribution of Fig. 2(d)(e)(f). Specifically, as the driving period increases, the subharmonics in the distribution become suppressed, and the output signal (the peak near $t_j/T_\Omega = 1$) increases in weight in the response. The SNR peak is reached when the collective jumps are fully synchronized with the drive, as an optimized peak emerges near $t_j/T_\Omega = 1$ and dominates the response. When the driving frequency is tuned past the resonance, multiple collective jumps can occur within a single driving period, leading to a deterioration of the signal and the SNR. Similar SNR behavior can be observed by fixing the driving period and tuning Ω_0 [see Fig. 3(b)]. As suggested by Fig. 1, this is equivalent to changing the intrinsic collective-jump rate to meet the resonance condition (indicated by the vertical dashed line). As such, emergent collective jumps assist the periodic drive to enhance the SNR in an open system, which is but the hallmark of the stochastic resonance.

Impact of many-body correlations. To understand the many-body nature of the collective quantum stochastic resonance, we consider a cluster model where interactions are treated exactly within the finite-size clusters, while mean-field approximations are adopted for inter-cluster interactions. For simplicity, we assume all clusters to have the same number of atoms M (dubbed the cluster size).

The overall density matrix can then be formally written as a direct product $\rho = \bigotimes_n \rho_n$, where ρ_n is the density matrix of the n th cluster. Apparently, quantum coherence and entan-

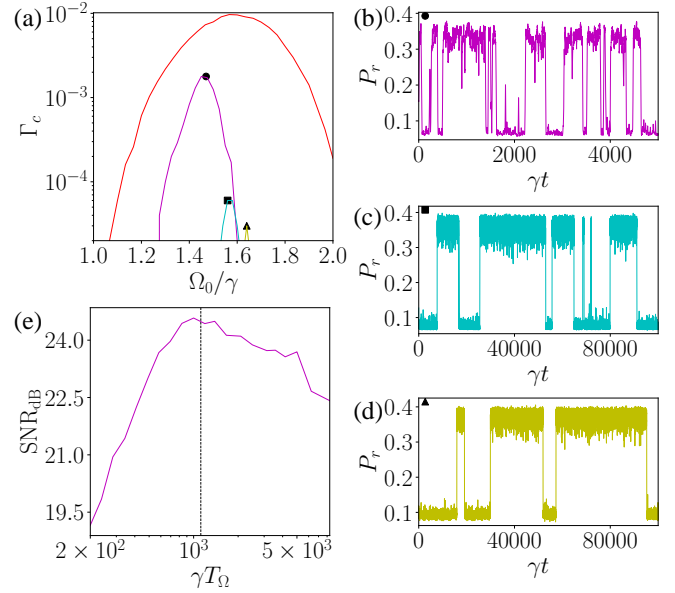


FIG. 4. (a) Intrinsic downward collective-jump rates as functions of Ω_0 under the cluster model in the absence of the periodic drive. The calculations are for a system of $N = 8$ atoms, with $M = 8$ (red), $M = 4$ (purple), $M = 2$ (blue), and $M = 1$ (yellow), respectively. (b)(c)(d) Single-trajectory dynamics for (b) $M = 4$ at $\Omega_0/\gamma = 1.47$, (c) $M = 2$ at $\Omega_0/\gamma = 1.56$, and (d) $M = 1$ at $\Omega_0/\gamma = 1.64$. The parameter Ω_0 is chosen at the position with the maximum Γ_c under any given M . (e) SNR under the cluster model of $M = 4$, with $\Omega_0/\gamma = 1.47$ and $A_\Omega/\gamma = 0.1$. The plotted SNR is averaged over 35 trajectories, where the evolution time for a single trajectory is $\gamma t = 50000$. The vertical dashed line indicates the theoretical resonance point, with $T_c \tilde{\Gamma}_c = 1$, corresponding to $\gamma T_c \approx 1118.4$. Other parameters are the same as those in Fig. 1.

glement only exist within the same cluster. While the master equation is formally the same as Eq. (1), the Hamiltonian of the n th cluster is

$$H_n = \sum_{j=1}^M \left[-\frac{\Delta}{2} (\sigma_{n,j}^z + 1) + \frac{\Omega}{2} \sigma_{n,j}^x \right] + \frac{V}{4} \sum_{j < k} (\sigma_{n,j}^z + 1) (\sigma_{n,k}^z + 1) + \frac{V}{4} \left(\sum_{m \neq n} P_r^m \right) \sum_{j=1}^M (\sigma_{n,j}^z + 1), \quad (6)$$

where $\sigma_{n,j}^{x,y,z}$ are the Pauli operators for the j th atom in the n th cluster, and the Rydberg excitation of the m th cluster is define as $P_r^m = \frac{1}{2} (\sum_{j=1}^M (\sigma_{m,j}^z + 1))$. Such a construction allows us to examine the impact of many-body correlations by decreasing the cluster size M , as the system is sequentially broken down into local clusters.

While the cluster model recovers the full-quantum description of Eq. (1) for $M = N$, the collective jumps are dramatically modified when $M < N$. Particularly, in the absence of the periodic modulation, the intrinsic collective-jump rate Γ_c significantly decreases for smaller M , as illustrated in Fig. 4(a). We also show the single-trajectory P_r for differ-

ent cluster sizes in Fig. 4(b)(c)(d), where the slowdown of the collective-jump rate with decreasing M is directly visible. This suggests that the resonance point should also shift toward lower frequencies at smaller M . We confirm this for $M = 4$ in Fig. 4(e), where the SNR peak occurs at a larger T_Ω than that of Fig. 3(a). Again, the SNR peak is close to the theoretical resonance position $T_c \bar{\Gamma}_c = 1$ (vertical dashed line).

Finally, we note that, in principle, the stochastic resonance persists even in the $M = 1$ case, albeit at a very small resonance frequency due to the scarcity of collective jumps. However, the quantum stochastic resonance does not exist under the optical Bloch equations of Eqs. (3) and (4), due to the complete lack of individual quantum jumps therein. Specifically, a key difference between the $M = 1$ cluster model and the full mean-field description is that, in the latter case, all the atoms are in the same state and described by the same density matrix. This renders sequential atomic emissions impossible, which is crucial for the buildup of a collective jump [30]. These observations clearly indicate the necessity of the emergent collective jumps and many-body correlations for the collective quantum stochastic resonance.

Discussion. We show that a collective quantum stochastic resonance occurs in dissipative Rydberg atoms, assisted by the emergent collective jumps that derive from the interplay of dissipation and Rydberg interactions. Key signatures of the resonance, such as the synchronized response and the enhanced SNR, are readily observable in arrays of Rydberg atoms confined to optical tweezers, or in Rydberg gases at low temperatures. As the temperature rises, the collective-jump rate decreases along with the size of local coherent clusters, and it would become more difficult to observe the resonance behavior. For thermal Rydberg gases whose dynamics are well-captured by the non-linear optical Bloch equations [33–35], neither the collective jump nor the quantum stochastic resonance persists. Nevertheless, based on the intrinsic non-linearity-induced bistability, stochastic resonances can still emerge when some form of classical noise is introduced [31]. The subsequent resonance behaviors would be similar in nature to those of conventional stochastic resonances, as well as related phenomena observed in non-linear non-Hermitian systems [40], but are fundamentally different from what we study here. Our findings establish quantum stochastic resonance in the many-body regime, and offer interesting possibilities for manipulating many-body quantum open systems, with potential applications in quantum-fluctuation-facilitated sensing.

We thank Zongkai Liu for helpful discussions. This work is supported by the National Natural Science Foundation of China (Grant No. 12374479) and the Innovation Program for Quantum Science and Technology (Grant No. 2021ZD0301200).

* These authors contributed equally to this work

† wyz@ustc.edu.cn

- [1] L. Gammaitoni, P. Hanggi, P. Jung, and F. Marchesoni, *Rev. Mod. Phys.* **70**, 223 (1998).
- [2] T. Wellens, V. Shatokhin, and A. Buchleitner, *Rep. Prog. Phys.* **67**, 45 (2004).
- [3] R. Benzi, A. Sutera, and A. Vulpiani, *J. Phys. A* **14**, L453 (1981).
- [4] J. K. Douglass, L. Wilkens, E. Pantazelou, and F. Moss, *Nature (London)* **365**, 337 (1993).
- [5] D. F. Russell, L. A. Wilkens, and F. Moss, *Nature (London)* **402**, 291 (1999).
- [6] B. McNamara, K. Wiesenfeld, and R. Roy, *Phys. Rev. Lett.* **60**, 2626 (1988).
- [7] A. Buchleitner and R. Mantegna, *Phys. Rev. Lett.* **80**, 3932 (1998).
- [8] S. F. Huelga and M. B. Plenio, *Phys. Rev. A* **62**, 052111 (2000).
- [9] A. Joshi and M. Xiao, *Phys. Rev. A* **74**, 013817 (2006).
- [10] J. Han, H. Liu, Q. Sun, N. Huang, Z. Wang, and S. Li, *Opt. Lett.* **40**, 5367 (2015).
- [11] K. J. H. Peters, Z. Geng, K. Malmir, J. M. Smith, and S. R. K. Rodriguez, *Phys. Rev. Lett.* **126**, 213901 (2021).
- [12] S. Fauve and F. Heslot, *Phys. Lett. A* **97**, 5-7 (1983).
- [13] K. Wiesenfeld, D. Pierson, E. Pantazelou, C. Dames, and F. Moss, *Phys. Rev. Lett.* **72**, 2125 (1994).
- [14] R. Löfstedt and S. M. Coppersmith, *Phys. Rev. Lett.* **72**, 1947 (1994).
- [15] D. E. Makarov and N. Makri, *Phys. Rev. B* **52**, R2257 (1995).
- [16] M. Grifoni and P. Hänggi, *Phys. Rev. Lett.* **76**, 1611 (1996).
- [17] K. Dong and N. Makri, *Phys. Rev. A* **70**, 042101 (2004).
- [18] S. F. Huelga and M. B. Plenio, *Phys. Rev. Lett.* **98**, 170601 (2007).
- [19] T. Wagner, P. Talkner, J. C. Bayer, E. P. Rugeramigabo, P. Hänggi, and R. J. Haug, *Nat. Phys.* **15**, 330-334 (2019).
- [20] M. Hänze, G. McMurtrie, S. Baumann, L. Malavolti, S. N. Coppersmith, and S. Loth, *Sci. Adv.* **7**, eabg2616 (2021).
- [21] M. Saffman, T. G. Walker, K. Mølmer, *Rev. Mod. Phys.* **82**, 2313 (2010).
- [22] A. Browaeys and T. Lahaye, *Nat. Phys.* **16**, 132 (2020).
- [23] M. D. Lukin, M. Fleischhauer, R. Cote, L. M. Duan, D. Jaksch, J. I. Cirac, and P. Zoller, *Phys. Rev. Lett.* **87**, 037901 (2001).
- [24] H. Bernien, S. Schwartz, A. Keesling, H. Levine, A. Omran, H. Pichler, S. Choi, A. S. Zibrov, M. Endres, M. Greiner, V. Vuletić, and M. D. Lukin, *Nature (London)* **551**, 579 (2017).
- [25] S. Ebadi, T. T. Wang, H. Levine, A. Keesling, G. Semeghini, A. Omran, D. Bluvstein, R. Samajdar, H. Pichler, W. W. Ho, S. Sachdev, M. Greiner, V. Vuletić, and M. D. Lukin, *Nature (London)* **595**, 227 (2021).
- [26] P. Scholl, M. Schuler, H. J. Williams, A. A. Eberharter, D. Barredo, K.-N. Schymik, V. Lienhard, L.-P. Henry, T. C. Lang, T. Lahaye, A. M. Läuchli, and A. Browaeys, *Nature (London)* **595**, 233 (2021).
- [27] D. Bluvstein, H. Levine, G. Semeghini, T. T. Wang, S. Ebadi, M. Kalinowski, A. Keesling, N. Maskara, H. Pichler, M. Greiner, V. Vuletić, and M. D. Lukin, *Nature (London)* **604**, 451 (2022).
- [28] T. Graham, Y. Song, J. Scott, C. Poole, L. Phuttitarn, K. Jooya, P. Eichler, X. Jiang, A. Marra, B. Grinkemeyer, M. Kwon, M. Ebert, J. Cherek, M. T. Lichtman, M. Gillette, J. Gilbert, D. Bowman, T. Ballance, C. Campbell, E. D. Dahl, O. Crawford, N. S. Blunt, B. Rogers, T. Noel, and M. Saffman, *Nature (London)* **604**, 457 (2022).
- [29] C. Chen, G. Bornet, M. Bintz, G. Emperauger, L. Leclerc, V. S. Liu, P. Scholl, D. Barredo, J. Hauschild, S. Chatterjee, M. Schuler, A. M. Laeuchli, M. P. Zaletel, T. Lahaye, N. Y. Yao, and A. Browaeys, *Nature (London)* **616**, 691 (2023).

- [30] T. E. Lee, H. Häffner, and M. C. Cross, *Phys. Rev. Lett.* **108**, 023602 (2012).
- [31] See Supplemental Material for details.
- [32] T. E. Lee, H. Häffner, and M. C. Cross, *Phys. Rev. A* **84**, 031402(R) (2011).
- [33] C. Carr, R. Ritter, C. G. Wade, C. S. Adams, and K. J. Weatherill, *Phys. Rev. Lett.* **111**, 113901 (2013).
- [34] N. Šibalić, C. G. Wade, C. S. Adams, K. J. Weatherill, and T. Pohl, *Phys. Rev. A* **94**, 011401(R) (2016).
- [35] N. R. de Melo, C. G. Wade, N. Šibalić, J. M. Kondo, C. S. Adams, and K. J. Weatherill, *Phys. Rev. A* **93**, 063863 (2016).
- [36] J. Dalibard, Y. Castin, and K. Mølmer, *Phys. Rev. Lett.* **68**, 580 (1992).
- [37] R. Dum, P. Zoller, and H. Ritsch, *Phys. Rev. A* **45**, 4879 (1992).
- [38] M. B. Plenio and P. L. Knight, *Rev. Mod. Phys.* **70**, 101 (1998).
- [39] P. Talkner, *Physica A* **325**, 124-135 (2003).
- [40] Z. Li, C. LI, G. Xu, W. Chen, Z. Xiong, H. Jing, J. S. Ho, and C.-W. Qiu, *Sci. Adv.* **9**, eadi0562 (2023).

Supplemental Material for ‘‘Collective quantum stochastic resonance in Rydberg atoms’’

In this Supplemental Material, we provide details on the calculation of the resonance condition, discussions on the finite-range Rydberg interactions, bistability under the cluster model and the condition for stochastic resonances within a mean-field framework.

The resonance condition

In the literature, the resonance condition for the stochastic resonance is often given as the matching between the driving frequency with the intrinsic noise-induced switching rate. In terms of the parameters defined in the main text, this condition corresponds to $T_\Omega \Gamma_c = 1$. Note that we define Γ_c as the rate of the downward collective jump, which differs from the total collective-jump rate by a factor of two. Furthermore, as demonstrated in Fig. 4(a) of the main text, Γ_c is a function of Ω_0 , and changes non-monotonically as the mean-field bistable region is traversed. While this reflects the many-body nature of the collective jumps, it also means that the intrinsic collective-jump rate varies as the Rabi frequency of the Rydberg excitation laser is driven around Ω_0 . To account for this variation, we use a path-averaged jump rate $\tilde{\Gamma}_c$ to estimate the resonance condition. Explicitly, we define

$$\tilde{\Gamma}_c = \frac{1}{T_\Omega} \int_0^{T_\Omega} \Gamma_c[\Omega(t)] dt. \quad (\text{S1})$$

We numerically evaluate $\tilde{\Gamma}_c$, and estimate the resonance positions in Fig. 3 and Fig. 4(e), which are close to the corresponding SNR peaks.

Spatial dependence of the Rydberg interactions

Throughout the main text, we model the Rydberg interactions through an all-to-all constant coupling. In reality, depending on the experimental condition, the Rydberg interactions can be dipolar, with $1/r^3$ spatial dependence (r is the interatomic distance), or Van-der-Waals-like, with $1/r^6$ spatial dependence. The collective quantum stochastic resonance studied in the main text persists even when considering the spatial dependence of the Rydberg interactions. To demonstrate this point, we study a one-dimensional chain of Rydberg atoms with $1/r^6$ interaction, where the many-body effects are much weaker than the dipolar type.

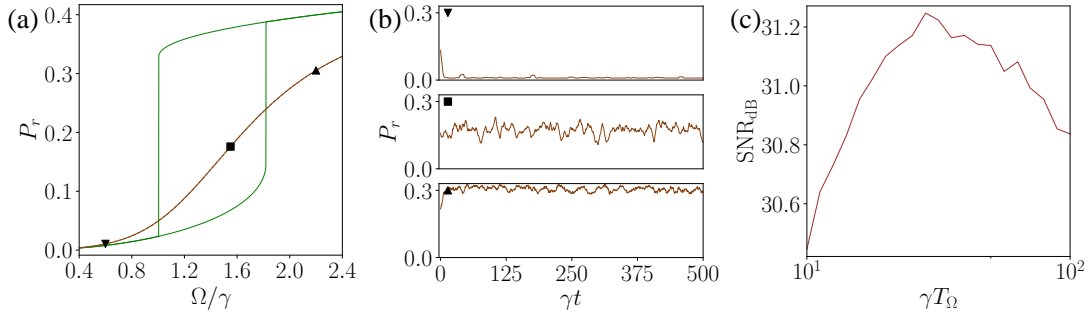


FIG. S1. Stochastic resonance with spatially dependent Rydberg interactions. (a) Rydberg-state population P_r in the steady state of the master equation (brown), and in the bistable states of the optical Bloch equations (green). (b) Single-trajectory dynamics. From top to bottom: $\Omega/\gamma = 0.6, 1.55, 2.2$, as indicated by the corresponding markers in (a). (c) SNR as a function of the modulation period with $\Omega_0/\gamma = 1.55$ and $A_\Omega/\gamma = 0.2$, averaged over 100 trajectories each with an evolution time $\gamma t = 10000$. For all figures, we take $N = 8$, with other parameters the same as those in Fig. 1 of the main text.

The interaction Hamiltonian is written as

$$H_{int} = \frac{945(N-1)V}{8\pi^6(j-k)^6} \sum_{j < k} (\sigma_j^z + 1)(\sigma_k^z + 1), \quad (\text{S2})$$

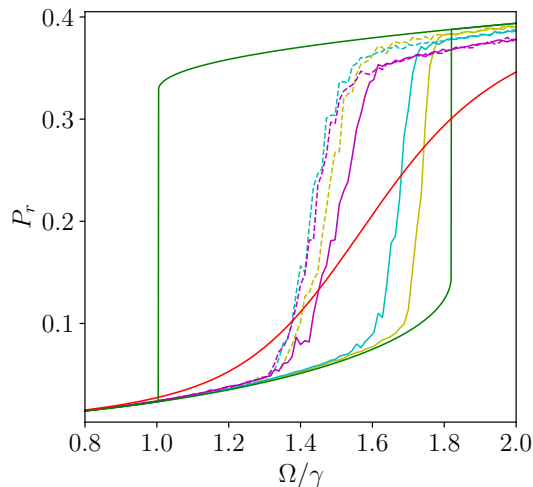


FIG. S2. Bistability with decreasing cluster size M . The population of the Rydberg state P_r is calculated by averaging 100 trajectories, each within the time $\gamma t \in [90, 100]$, where the system has relaxed to the vicinity of the steady state. We take $N = 8$, and apply the cluster model with $M = 4$ (purple), $M = 2$ (blue), and $M = 1$ (yellow), for two distinct initial Rydberg-state populations: $P_r = 0.1$ (solid), and $P_r = 0.6$ (dashed). The red and green curves are the same as those in Fig. 1 of the main text, indicating the steady-state solutions of the full quantum and mean-field models, respectively.

where we take a dimensionless lattice constant. To facilitate comparison with the mean-field results, the coefficients are determined such that the non-linear detuning term in the optical Bloch equation [Eq. (4) in the main text] can be derived from Eq. (S2) once a mean-field approximation is applied.

In Fig. S1, we show the numerical results for the steady states, the quantum trajectories, and the SNR. The emergence of collective jumps in the middle panel of Fig. S1(b) and the peaked SNR in Fig. S1(c) indicate the persistence of the collective quantum stochastic resonance. Compared to the middle panel in Fig. 1(c), the signals for the collective jumps are less prominent here, which we attribute to the reduction in the long-range correlations under the interaction in Eq. (S2).

Bistability under the cluster model

The cluster model we introduce in the main text acquires non-linear inter-cluster interactions for $M < N$. This gives rise to bistability-like behaviors at long times, reminiscent of the results under the full mean-field treatment [green curves in Fig. 1(b) of the main text].

To illustrate this point, we numerically evolve the system to the vicinity of its long-time steady state, using the quantum-trajectory scheme under the cluster model. The ensemble averaged P_r for different initial states are shown in Fig. S2, which suggests the presence of a bistable region. Specifically, similar to the full mean-field case, initial states with distinct Rydberg populations evolve to final states with distinct Rydberg populations. The hysteresis in the Rydberg population P_r outlines the region with bistability-like behaviors at long times. Clearly, with decreasing cluster size M , the bistable region is significantly enlarged, but still lies within the mean-field bistable regime. Combined with the results in Fig. 4 of the main text, we conclude that, with decreasing M , the increasingly dominant bistable physics is accompanied by the reduction in the collective-jump rate, both closely related to the gradual breakdown of the long-range quantum correlations.

Classical stochastic resonance under the mean-field model

The cluster model we introduce in the main text acquires non-linear inter-cluster interactions for $M < N$. This gives rise to bistability-like behaviors at long times, reminiscent of the results under the full mean-field treatment [green curves in Fig. 1(b) of the main text].

To illustrate this point, we numerically evolve the system to the vicinity of its long-time steady state, using the quantum-trajectory scheme under the cluster model. The ensemble averaged P_r for different initial states are shown in Fig. S2, which suggests the presence of a bistable region. Specifically, similar to the full mean-field case, initial states with distinct Rydberg populations evolve to final states with distinct Rydberg populations. The hysteresis in the Rydberg population P_r outlines the

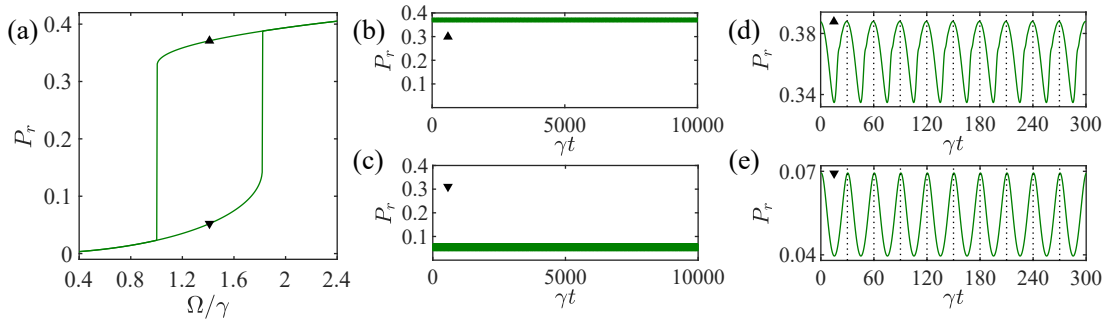


FIG. S3. Dynamics of the Rydberg-state population under the optical Bloch equations, with a periodic drive but without classical noise. (a) Rydberg-state populations in the bistable states. The bistable solutions exist in the range $\Omega/\gamma \in [1.0042, 1.8195]$. (b)(c) Dynamics of the Rydberg-state population, when the system is initialized in different steady states (indicated by the black markers). (d)(e) Enlarged view of the dynamics in (b)(c), respectively, at short times. The parameters are $\Omega_0/\gamma = 1.413$, $A_\Omega/\gamma = 0.39$, and $\gamma T_\Omega = 30$. Other parameters are the same as those in Fig. 1 of the main text.

region with bistability-like behaviors at long times. Clearly, with decreasing cluster size M , the bistable region is significantly enlarged, but still lies within the mean-field bistable regime. Combined with the results in Fig. 4 of the main text, we conclude that, with decreasing M , the increasingly dominant bistable physics is accompanied by the reduction in the collective-jump rate, both closely related to the gradual breakdown of the long-range quantum correlations.

Classical stochastic resonance under the mean-field model

In this section, we show that, under the full mean-field model of Eqs. 3 and 4, the collective quantum stochastic resonance does not occur due to the complete lack of collective jumps. Nevertheless, a classical stochastic resonance can appear if some form of classical noise is introduced. The underlying mechanism of such a stochastic resonance is fundamentally different from that of the collective quantum stochastic resonance discussed in the main text.

In Fig. S3, we show the Rydberg-state population dynamics given by Eqs. (3) and (4), under a periodic modulation of the Rabi frequency $\Omega(t) = \Omega_0 + A_\Omega \cos(2\pi t/T_\Omega)$. We choose a $\Omega_0/\gamma = 1.413$ within the non-linearity-induced bistable region, as shown in Fig. S3(a). In Fig. S3(b)(c), we show the time-evolved $P_r = \bar{\rho}_{rr}$ when the density matrix is initialized in the steady state with high (b) or low (c) Rydberg populations, respectively. Under the periodic drive, the population features oscillations (at the driving frequency) around the initial steady-state value [see Fig. S3(d)(e)], but there are no signs of collective jumps between the two values. Note that, similar to the condition in the main text (and indeed with the common practice in the classical stochastic resonance), we focus on the weak-signal case, where the periodically modulated $\Omega(t)$ does not cross the boundary of the bistable region. This means that $(\Omega_0 \pm A_\Omega)/\gamma \in [1.0042, 1.8195]$.

We now introduce a noise term to the drive, with $\Omega(t) = \Omega_0 + A_\Omega \cos(2\pi t/T_\Omega) + \sqrt{D}\zeta(t)$. Here the term $\sqrt{D}\zeta(t)$ describes white noise with zero mean and a variance of D . Numerically the white noise is generated by creating a signal consisting of N data points, where each point is sampled from a normal distribution with zero mean and a standard deviation of \sqrt{D} . The resulting discrete white-noise signal is then interpolated over the evolution time interval $[0, T_r]$ to obtain a continuous function. The range of the noise in the frequency domain is $[0, N/T_r]$. In Fig. S4(a), we show the time-evolved $P_r = \bar{\rho}_{rr}$ without any averaging over the white noise. The collective state-switching is now visible, as well as the subharmonics in the distribution of inter-jump intervals p_j , as we show in In Fig. S4(b). Crucially, the occurrence of the state switching is due to the fact that, with the addition of noise, the system acquires a finite probability to cross both boundaries of the bistable region. The underlying mechanism is therefore fundamentally different from the emergent collective jumps in the main text. Again, these emergent collective jumps derive from the interplay of dissipation and Rydberg interactions: they hinge upon the consecutive quantum jumps of individual atoms, and are further facilitated by the interaction-induced quantum entanglement between atoms.

Correspondingly, in Fig. S4(c)(d), we show the numerically calculated SNR as functions of the driving period and the noise strength \sqrt{D} , respectively. In both cases, a peak in the SNR can be identified, signaling the stochastic resonance point. Particularly, the result in Fig. S4(d) is an exemplary case of the classical stochastic resonance, where the periodic drive and noise conspire to drive the system over the threshold (bistable boundary here), leading to optimized state switching at the resonance point.

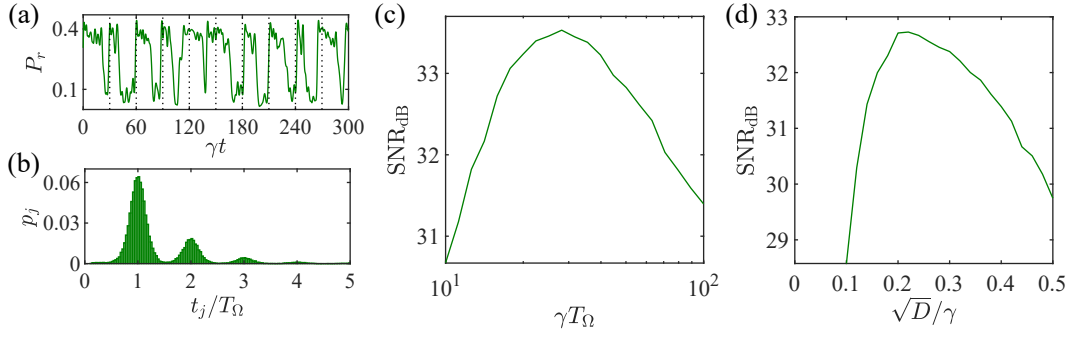


FIG. S4. Classical-noise-induced state switching and stochastic resonance. (a) Dynamics of Rydberg-state population under a periodic drive with white noise. The standard deviation of the noise is $\sqrt{D}/\gamma = 0.4$ and the range of the noise in the frequency domain is $[0, \gamma]$. (b) Distribution of the inter-jump intervals within the evolution time $\gamma t \in [0, 1.6 \times 10^6]$. (c) The SNR as a function of T_Ω . (d) The SNR as a function of \sqrt{D} , for $\gamma T_\Omega = 100$. The parameters are $\Omega_0/\gamma = 1.413$, $A_\Omega/\gamma = 0.39$, other parameters are the same as those in Fig. 1 of the main text. The curves in both (c) and (d) represent the average of 120 trajectories, each with an evolution time of $\gamma t = 10000$.